Journal of Alloys and Compounds 375 (2004) 162–170

Journal of ALLOYS AND COMPOUNDS

www.elsevier.com/locate/jallcom

Reaction kinetics and phase diagram studies in the Ti–Zn system

G.P. Vassilev [a,*], X.J. Liu [b], K. Ishida [b]

[a] *University of Sofia, Faculty of Chemistry, J. Bourchier Avenue 1, 1164 Sofia, Bulgaria*
[b] *Department of Materials Science, Graduate School of Engineering, Tohoku University, Aoba-yama 02, Sendai 980-8579, Japan*

Received 12 October 2003; received in revised form 11 November 2003; accepted 20 November 2003

Abstract

Ti–Zn phase diagram and layers growth kinetics, have been studied at 500, 600 and 900 °C. Linear growth has been observed. The calculated values of the growth constants K_G are: at 500 °C, $K_G = (7.5 \pm 0.3) \times 10^{-9}\,\mathrm{m\,s^{-1}}$; at 600 °C, $K_G = (8.0 \pm 0.2) \times 10^{-9}\,\mathrm{m\,s^{-1}}$.

An indication about the presence of a formerly unknown compound (Ti_2Zn_3) has been found out by electron microprobe analyses and optical microscopy.

Homogeneity ranges (probably metastable) have been observed for some phases that are considered to be stoichiometric.

Keywords: Transition metals alloys; Intermetallics; Phase diagram; Layers growth

1. Introduction

The technological importance of the Ti–Zn system has been recognized since 1912 due to the use of titanium additions for grain refinement at zinc casting. Recently, Leone et al. [1,2] found that Ti promotes creep resistance in rolled alloys. The Ti–Zn alloys are currently used also for metal coatings pigmentation [3] and for controlling the coatings' thickness when galvanizing silicon steels [4,5].

Lately this system is interesting in connection with the prospective use of both Ti and Zn additions in multicomponent solders [6].

Nevertheless the Ti–Zn phase diagram is not well studied [7–10]. The interaction kinetics between liquid Zn and solid Ti is entirely unknown. Thus the purpose of this work is to study the reaction kinetics between liquid zinc and titanium as well as the Ti–Zn phase diagram.

2. Information on the Ti–Zn phase diagram

The system Ti–Zn has been studied by numerous researchers [11–21]. Description of the phases relevant to the Ti–Zn system is exhibited in Table 1. In Fig. 1 we present a Ti–Zn phase diagram based on the assessment of Murray [8] and Massalski [10]. Data recently reported by Ono et al. [21] about the Ti-rich side of the system are included also.

Contradictions about the Zn-rich part of the system subsist. For example, Murray [8] and Massalski [10] assume that the most Zn-rich phase is $TiZn_{15}$, while other authors [24,25] have found that its formula is $TiZn_{16}$. According to Massalski [10], the compound $TiZn_3$ melts peritectically at 923 K. Nevertheless Heine and Zwicker [16] suggested that this binary phase is stable until around 1173 K.

Chen et al. [25] studied the crystal structure of Ti_3Zn_{22} (according to them with exact composition $Ti_{0.114}Zn_{0.886}$). They have not observed any other phases between $TiZn_3$ and (ηZn) (the parenthesis indicate a phase, to be distinguished from the respective element). However, various authors supposed the existence, in this concentration interval, of other phases such as $TiZn_{10}$ [12] or as $TiZn_5$ [16]. Moreover, Gloriant et al. [4] have found that another compound ($TiZn_7$) is the only phase between $TiZn_{15}$ and $TiZn_3$.

Contentious are the data about the invariants and the liquidus line [11,12,16,18]. At least six invariants are observed in the composition range 50–100 at.% Zn but the interpretations differ greatly.

The shape of the liquidus is unknown too. According to one group of authors [11,12,18] the liquidus rises steeply, reaching 600 °C at about 97 at.% Zn. Contrary, the liquidus points of Heine and Zwicker [16] lie considerably lower in temperature.

* Corresponding author. Tel.: +359-2938-1023; fax: +359-296-25-438.
E-mail address: gpvassilev@excite.com (G.P. Vassilev).

0925-8388/$ – see front matter © 2003 Elsevier B.V. All rights reserved.
doi:10.1016/j.jallcom.2003.11.026

Table 1
Description of the phases relevant to the Ti–Zn system [7,10,22,23]

Phase	Approx. concentration interval	Pearson symbol	Space group	Prototype	Source
(ηZn)	≈100 at.% Zn	hP2	*P*6$_3$/*mmc*	Mg	
(αTi)	≈100 at.% Ti	hP2	*P*6$_3$/*mmc*	Mg	
(βTi)[a]	≈100–80 at.% Ti	CI2	*Im*$\bar{3}$*m*	W	
$TiZn_{16}$[b]	94.12 at.% Zn	–	*Cmcm*	$TiZn_{16}$	[24,25]
$TiZn_{15}$[b]	93.75 at.% Zn	OC68	*Cmcm*	$TiZn_{15}$	[10]
$TiZn_{10}$	90.91 at.% Zn	–	–	Distorted γ-brass	[17]
$TiZn_8$	88.89 at.% Zn	–	–	–	[26]
Ti_3Zn_{22}[c]	88.6 at.% Zn	–	*P*4$_2$/*mbc*	Ti_3Zn_{22}	[25]
$TiZn_7$	87.50 at.% Zn	–	–	–	[4]
$TiZn_5$	83.33 at.% Zn	–	–	–	[16]
$TiZn_3$	25.0 at.% Ti	cP4	*Pm*$\bar{3}$*m*	$AuCu_3$	[13,27]
Ti_2Zn_3[d]	40 at.% Zn	–	–	–	This work
$TiZn_2$	33.3 at.% Ti	hP12	*P*6$_3$/*mmc*	$MgZn_2$ (Laves phase)	[13]
TiZn	50.0 at.% Ti	cP2	*Pm*$\bar{3}$*m*	CsCl	[16]
Ti_2Zn	66.7 at.% Ti	tI6	*I*4/*mmm*	$MoSi_2$	[14,28]

[a] High-temperature form.
[b] In this work both formulae are assumed to appertain to one single phase $TiZn_{16}$.
[c] Might appertain to the phase $TiZn_7$ or to the phase $TiZn_8$ (one common phase with limited homogeneity range could not be excluded neither).
[d] In the compilation [22] Heine and Zwicker [16] are cited; nevertheless this compound is not mentioned in their original work. We think that there is a printing error in [22] (confusion with $TiZn_3$).

The thermodynamic properties of the Zn–Ti alloys have not been studied experimentally. Nevertheless, the Miedema model calculations indicate large negative deviations relative to the ideal solutions formation [29].

3. Experimental

3.1. Experimental procedures

The phase and chemical composition of diffusion couples and equilibrated alloys annealed at 500 and 600 °C have been investigated. Studies have been performed by electron probe microanalyses (EPMA) making use of the wave disperse system (WDS) method with consecutive determination of the elements' concentration, optical microscopy

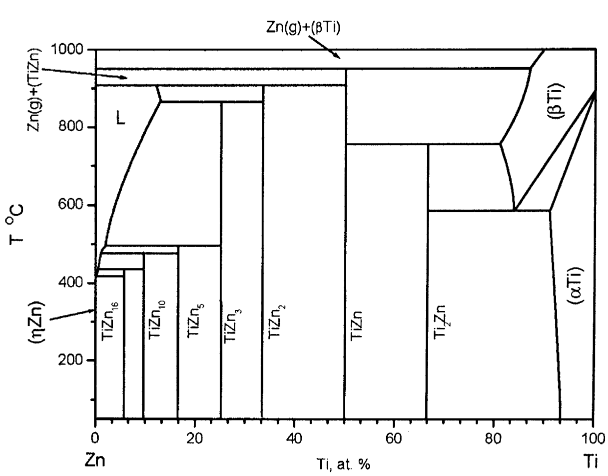

Fig. 1. The Ti–Zn phase diagram. Authors' compilation based on the assessments of Murray [8] and Ono et al. [21]. The invariants' temperatures are approximate.

and differential scanning calorimetry. The exact chemical composition of some alloys (after annealing) was obtained through atomic emission spectroscopy by inductively coupled plasma (AES-ICP) analyses.

Diffusion couples with end-members constituted of bulk arc-melted Ti (cut as rectangular pieces) and pure Zn shots (3N) have been used. For this purpose, weighted quantities of both metals have been put in quartz tubes, rinsed three times with pure argon, and sealed under vacuum of 0.4 Pa. After pertinent isothermal annealing (Tables 2–5), the specimens have been quenched in ice water. Thereafter they have been cut, usually, normally to the solid/liquid interface. The concentration profiles of the layers grown in the diffusion zone as well as the compositions of the phases in the volume of the liquid end-member have been found by EPMA. Optical microscopy has been used for the phase identification and the determination of the layer thickness also. The optical microscope studies have been done after etching the polished surfaces with mixtures of 25 parts concentrated HNO_3, 25 parts HF (40%) and 50 parts glycerin ($C_3H_5(OH)_3$) or 50% $C_3H_5(OH)_3$ and 50% concentrated HCl.

As mentioned above, the laboratory syntheses of these Ti containing alloys have been done using quartz (SiO_2) tubes. Nevertheless the standard Gibbs free energy of the TiO_2 has larger negative values than that of the SiO_2 [30]. Consequently the pure titanium can act as reducing agent on the silicon dioxide leading to changes of the specimens' compositions.

Another specific problem is the large oxygen solubility in (αTi) [10] that is possible source of oxygen contamination. The oxygen forms interstitial solutions with the hexagonal (αTi). For these reasons, the specimens have been regularly analyzed by electron probe microanalyses (EPMA) for Ti, Zn, Si and O.

Table 2
Results of the reaction kinetics studies at 773 K

No.	Δx (m) $\times 10^{-6}$	Phases	t (s) $\times 10^3$	Note
1	20–65 n.a.	Liq (0.990–0.997); $TiZn_5$? or $TiZn_3$ (0.804–0.762); Ti_2Zn_3 (0.593–0.575); TiZn (0.52); (α Ti, Zn) (0.042–0.00)	1.8	Not used for growth constant determination because the layer has not constant thickness yet. $R1 = 27\%$. Step = 1
2	55	Liq (0.99); $TiZn_7$ (0.885–0.874); $TiZn_3$ (0.73–0.72); (αTi) (0.00)	3.6	$R1 = 43\%$. Step = a.s.
3	n.a.	Liq (0.98); $TiZn_7$ (0.863–0.857); $TiZn_5$? (0.83); $TiZn_3$ (0.75–0.73); $TiZn_2$ (0.69); Ti_2Zn_3 (0.62–0.60); TiZn (0.57–0.51); (αTi,Zn) (0.04–0.00)	3.6	Step 0.5×10^{-6} m; compositions $TiZn_{16}$ and $TiZn_{10}$ found in the liquid phase next to the layer. $R1 = 39\%$ section, parallel to the solid/liquid interface
4	90	Liq (0.99); $TiZn_7$ (0.886–0.851); $TiZn_3$ (0.72); (αTi,Zn) (0.09–0.00)	7.2	$R1 = 28\%$. Step = a.s.
5	96	Liq (0.98); $TiZn_7$ (0.88); $TiZn_5$ or $TiZn_3$? (0.79); Ti_2Zn_3 (0.61); (αTi) (0.00)	10.8	$R1 = 42\%$. Step = a.s.
6	140	Liq (0.98); $TiZn_7$ (0.879–0.860); $TiZn_5$? (∼0.84); $TiZn_3$ (0.813–0.762); Ti_2Zn (0.375); (αTi,Zn) (0.081–0.000)	14.4	$R1 = 43\%$. Step = 10×10^{-6} m
7	n.a.	Liq (0.95); $TiZn_{5(4)}$? or $TiZn_3$ (0.81–0.80); Ti_2Zn_3 (0.622); (αTi,Zn) (0.0)	21.6	Step = a.s. Braking of the layers is observed (see Fig. 2)
8	640	Liq (0.98); $TiZn_7$ (0.872–0.868); $TiZn_3$? (0.79); $TiZn_3$ (0.73–0.70); $TiZn_2$ (0.70–0.667); (αTi,Zn) (0.031–0.000)	57.6	$R1 = 26\%$. Steps = 1, 2 and 10×10^{-6} m
9	770	Liq (0.98)[a]; $TiZn_7$ (0.868); $TiZn_3$ (0.72); $TiZn_2$ (0.68); (αTi,Zn) (0.027–0.000)	86.4	$R1 = 21\%$. Step = a.s.
10	1350	Liq (0.98)[a]; $TiZn_7$ (0.880); $TiZn_{5(4)}$? (0.80); $TiZn_3$ (0.75–0.71); $TiZn_2$ (0.70–0.68); Ti_2Zn_3 (0.594); (αTi,Zn) (0.03–0.00)	180	$R1 = 19\%$. Step = a.s.

No.: specimen's number; Δx ((m) $\times 10^{-6}$): total thickness of the reaction diffusion layers (the underlined formula indicates the predominant phase(s) for the pertinent specimen. The concentration intervals of the pertinent phases, as measured by EPMA are shown in the parentheses) grown normally to the solid/liquid interface; t (s): annealing time; n.a.: not appropriate (the thickness of the corresponding layer has not been used for calculations); step ((m) $\times 10^{-6}$): distance between the points where EPMA analyses have been done; a.s.: arbitrary step (manually chosen points); phases (the lack of a possible Ti–Zn phase, in this column, does not imply it is absent in the diffusion layer): compounds identified in the diffusion zone. $R1$: ratio (%) between the first layer thickness and Δx.

[a] Considered to be liquidus points.

Table 3
Results of the reaction kinetics studies at 873 K

No.	Δx (m) $\times 10^{-6}$	Phases	t (s) $\times 10^3$	Note
11	n.a.	Liq (1.00–0.98); $TiZn_7$ (0.88); $TiZn_5$? And/or $TiZn_3$ (0.80–0.67); Ti_2Zn_3 (0.60); (αTi,Zn) (0.13–0.00)	0.9	The first layer is of Ti_2Zn_3, the second—mainly of $TiZn_3$ (inclusions of $TiZn_2$ are observed also), the third (thin, adjacent to the liquid)—$TiZn_7$. Step = 1 and 3×10^{-6} m
12	150	Liq (0.98); $TiZn_7$ (0.878–0.874); $TiZn_3$ (0.745–0.725); (αTi,Zn) (0.13–0.00)	3.6	$R1 = 43\%$. Step = a.s.
13	200	Liq (0.97); $TiZn_8$ (0.894); $TiZn_7$ (0.879); $TiZn_3$ (0.746–0.728); Ti_2Zn_3 (0.62); TiZn (0.46); Ti_3Zn (0.26); Ti_2Zn (0.35); (αTi) (0.00)	10.8	$R1 = 44\%$. Step = a.s.
14	212	Liq (0.99); $TiZn_7$ (0.878–0.875); $TiZn_3$ (0.737–0.735); (αTi) (0.00)	14.4	In the former liquid phase, $TiZn_{16}$ dendrites are observed. $R1 = 44\%$. Step = 15
15	250	Liq (0.98); $TiZn_7$ (0.875); $TiZn_5$? (0.835); $TiZn_3$ (0.740–0.724); (αTi,Zn) (0.01–0.00)	18.0	$TiZn_3$ crystals, surrounded by areas with composition corresponding to $TiZn_7$ are observed in the former liquid phase. $R1 = 48\%$. Step = a.s.
16	800	Liq (0.95)[a]; $TiZn_7$ (0.88); $TiZn_3$ (0.733); (αTi) (0.00)	86.4	$R1 = 43\%$. Step = 10 and 20×10^{-6} m
17	4000 n.a.	Liq (0.96)[a]; $TiZn_7$ (0.88); $TiZn_3$ (0.74); $TiZn_2$ (0.67); (αTi) (0.0)	180	The $TiZn_7$ layer is extremely porous and some fissures are observed. Well shaped $TiZn_7$ crystals are formed in the liquid phase. $R1$ = n.a. Step = a.s.

No.: specimen's number; Δx ((m) $\times 10^{-6}$): total thickness of the reaction diffusion layers (the underlined formula indicates the predominant phase(s) for the pertinent specimen. The intermetallic layer adjacent to the titanium-based solid solution (αTi,Zn) is always referred as first. In the parentheses the concentration intervals of the pertinent phases, as measured by EPMA are shown) grown normally to the solid/liquid interface; t (s): annealing time; n.a.: not appropriate (the thickness of the corresponding layer has not been used for calculations); step ((m) $\times 10^{-6}$): distance between the points where EPMA analyses have been done; a.s.: arbitrary step (manually chosen points); phases (the lack of a possible Ti–Zn phase, in this column, does not imply it is absent in the diffusion layer) compounds identified in the diffusion zone. $R1$: ratio (%) between the first layer thickness and Δx.

[a] Considered to be liquidus points (see Fig. 9).

Table 4
Results of the reaction kinetics studies at 1173 K

No.	Δx (m) $\times 10^{-6}$	Phases	t (s) $\times 10^{3}$	Note
18	27	Liq (0.94–0.93); $TiZn_3$ (0.72–0.71); TiZn (0.507); Ti_2Zn (0.347); (βTi,Zn) (0.17–0)	3.6	Monophase diffusion of Zn into (βTi) is registered. The maximal concentration is X_{Zn} = 0.17. Step = 2×10^{-6} m
19		Liq (0.95–0.92); crystals of $TiZn_3$ (0.75) and $TiZn_5$? or $TiZn_7$? (0.855) in the liquid	1.8	Si-containing layer (approx. Ti_5SiZn_4) along the tube's wall is found
20		Liq (0.95–0.92); crystals of TiZn (0.50) and $TiZn_3$ (0.75) in the liquid	3.6	Si-containing layer along the tube's wall is found. Ti_2Zn_3 and $TiZn_3$ layers have grown

No.: specimen's number; Δx ((m) $\times 10^{-6}$): total thickness of the reaction diffusion layers grown normally to the solid/liquid interface; t (s): annealing time; n.a.: not appropriate (the thickness of the corresponding layer has not been used for calculations); step ((m) $\times 10^{-6}$): distance between the points, where EPMA analyses have been done; a.s.: arbitrary step (manually chosen points); phases: compounds identified in the diffusion zone.

The first EPMA studies (wave disperse system method) revealed a correlation between the zinc and the oxygen contents that was difficult to explain. We looked in details for the reason and we found that there is an overlapping between the analytical oxygen $K_{\alpha,1}$ peak (70.432 mm) and the $L_{\alpha,1}$ peak of the Zn (73.080 mm). Furthermore care has been taken to calibrate the apparatus in order to minimize this effect. Finally, the following conditions have been used: Zn–LIF crystal, $K_{\alpha,1}$ peak (position 99.884 mm); Ti–PETJ crystal, $K_{\alpha,1,2}$ peak (position 88.033 mm); O–LDE2 crystal, $K_{\alpha,1}$ peak (position 70.432 mm); Si–TAP crystal, $K_{\alpha,1}$ peak (position 77.468 mm).

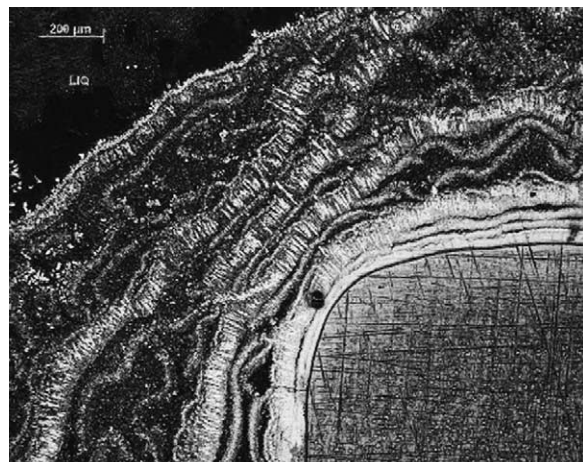

Fig. 2. Optical micrograph of diffusion couple no. 7 (annealed 6 h at 773 K) illustrating the breaking of the diffusion layers. The black area is the Liquid phase, the gray area (right-down angle) is (αTi).

3.2. Studies of the layers growth kinetics

As the reaction kinetics between Zn and Ti was unknown initially, some specimens have been annealed for 96 h at 1173 and 1073 K. We found that the Ti pieces are completely dissolved and large quantities of a compound corresponding

Table 5
Results obtained from specimens, where fast reaction occurred

No.	Observations	t (s) $\times 10^{3}$	Note
21[a]	Crystals of $TiZn_3$ (0.716 ± 0.003) in white matrix phase, probably, $TiZn_5$? and $TiZn_7$ (0.83–0.88)	7.2	Overall composition: X_{Zn} = 0.855
22[a]	Liquid phase (0.99–0.97) containing crystals of $TiZn_3$ (0.78)	21.6	Small undissolved Ti particle, surrounded by layers of Ti_2Zn_3 (0.595) and $TiZn_3$ (0.782)
23[a]	In the volume of the former liquid phase a white Zn-rich matrix (0.91–0.85) is observed, with crystals of $TiZn_3$ (predominant) and Ti_2Zn_3	21.6	Small undissolved Ti particle, layer of $TiZn_3$ (0.715). Specimen's composition: X_{Zn} = 0.831 ± 0.001 (by ICP)
24[a]	Predominant phase is Ti_2Zn_3; $TiZn_7$, $TiZn_3$ and $TiZn_2$ crystals are observed also	1.8	Small undissolved Ti particle, layers of Ti_2Zn_3 and $TiZn_7$. Specimen's composition: X_{Zn} = 0.800 ± 0.001 (by ICP)
25[a]	Crystals of Ti_2Zn_3 (see Fig. 5) are predominant. $TiZn_3$ crystals are observed also. The composition of the matrix phase (probably melted) is close to $TiZn_8$	28.8	Small undissolved Ti particle, where layers of Ti_2Zn_3 and $TiZn_7$ have grown
26[a]	Crystals of Ti_2Zn_3 (0.60), $TiZn_3$ and white matrix phase $TiZn_7$ (0.875)	57.6	Small undissolved Ti particle, layers of Ti_2Zn_3 and $TiZn_7$. Specimen's composition: X_{Zn} = 0.866 ± 0.001 (by ICP)
27[b]	$TiZn_7$ (0.874 ± 0.001); $TiZn_{5(4)}$? or $TiZn_3$ (0.799 ± 0.003)	30 d	Specimen's composition: X_{Zn} = 0.885 ± 0.001 (by ICP)

The numbers in the parentheses show the Zn mole fractions of the pertinent phase, as measured by EPMA, T (K): annealing temperature, t (s): annealing time. X_{Zn}: mole fraction of Zn.

[a] T = 873 K.

[b] T = 773 K.

to the stoechiometry Ti_2Zn_3 (containing also from 0 to 1 at.% Si) formed. The liquid phase consisted of almost pure zinc (with very feeble content of Ti and Si, while no oxygen rich-phases have been registered). The silicon was bounded in zinc containing extensions of the binary phases Ti_3Si and Ti_5Si_3. These specimens have not been used furthermore and shorter annealing times have been used in the further studies.

The experimental results about the growth kinetics of Ti–Zn reactionary layers at 773, 873 and 1173 K are compiled in Tables 2–4, respectively. In a number of experiments at 873 and 1173 K unusually fast reaction between (αTi) and melted Zn occurred. It resulted, usually, in an almost complete dissolution of the pure Ti. We have observed in some cases many fissures (Fig. 2) in the diffusion zone, allowing to the liquid Zn to enter in direct contact with (αTi) (i.e. a convection phenomenon appears, bypassing the diffusion through the intermediate layers). That is why we suppose that the reason for the fast reaction is the breaking of the diffusion layers, due to the weak adherence of the

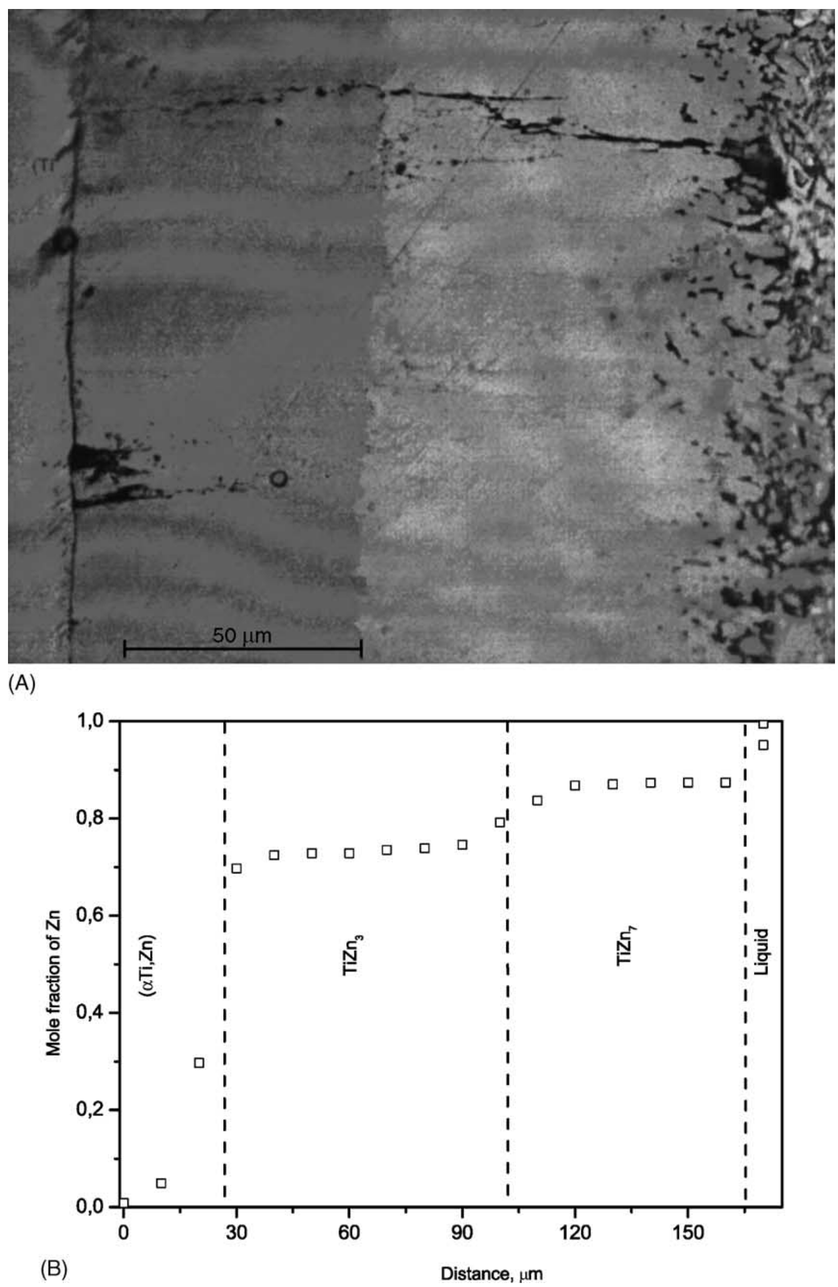

Fig. 3. (A) Optical micrograph of diffusion couple no. 6 (annealed 4 h at 773 K). Diffusion layers have grown between pure titanium (left), and the Liquid phase (right). The dark layer adjacent to (αTi) is constituted of $TiZn_3$, while the light one–of $TiZn_7$. (B) Concentration profile of diffusion couple no. 6 (annealed 4 h at 773 K), obtained by electron probe microanalyses. The diffusion zone is constituted mainly of two intermediate layers, identified as $TiZn_3$ and $TiZn_7$. The dashed lines represent visible interfaces.

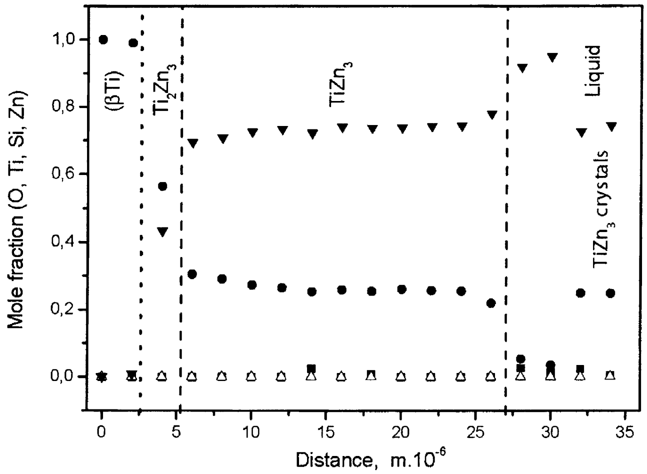

Fig. 4. Composition profiles (obtained by electron probe microanalyses) of diffusion couple no. 20, annealed 1 h at 1173 K. The symbols Δ, ●, ▼ and ■ denote the measured mole fractions of the elements Si, Ti, Zn and O, respectively. The dashed lines represent visible interfaces, the dotted line stays for the interface between the diffusion layers and (βTi) that could not be observed. The main layer consist of $TiZn_3$. Crystals of the latter compound are found in the Liquid phase as well.

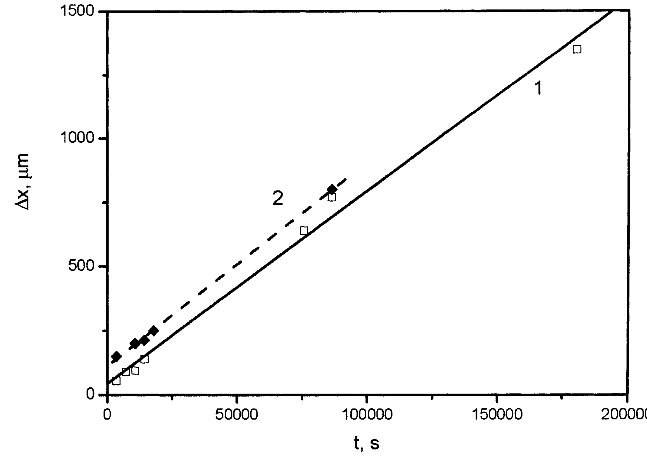

Fig. 6. Thickness (Δ*x*, μm) of the intermediate Ti–Zn layers as a function of the reaction time (*t*, s) at 500 °C (□, line 1) and 600 °C (Λ, line 2).

Ti–Zn diffusion layers among them. The results from the investigations of these specimens are exhibited in Table 5.

We found also that the total widths of the diffusion zones differ according to whether layers grow normally to the solid/liquid surface or along it. In the latter case, the layers thickness is lesser, that can be explained with the limited Zn diffusion flux.

Typically, two layers contribute effectively to the diffusion zone width. Other layers, when they appear are usually quite thin. Optical micrograph of diffusion couple no. 6 is shown in Fig. 3A. The concentration profile obtained by EPMA is exposed in Fig. 3B. In this example (specimen no. 6, Table 2), the main layers are $TiZn_3$ and $TiZn_7$. Between them a transition zone exists, that might correspond to $TiZn_5$ but a clear interface could not be observed. A thin layer of Ti_2Zn adjacent to (αTi) is found also.

Concerning the argued phase $TiZn_5$, we have found compositions indicating its presence (specimens nos. 3, 6–8, 10, 15, 27, see Tables 2–4). Nevertheless, we could not observe well-shaped interfaces separating these areas from other layers.

The studies at 900 °C, show that $TiZn_3$ forms directly from the Liquid phase. Concentration profile of specimen no. 20 (Table 4) is shown in Fig. 4. In this specimen a thin layer corresponding to the formula Ti_2Zn_3 has been observed,

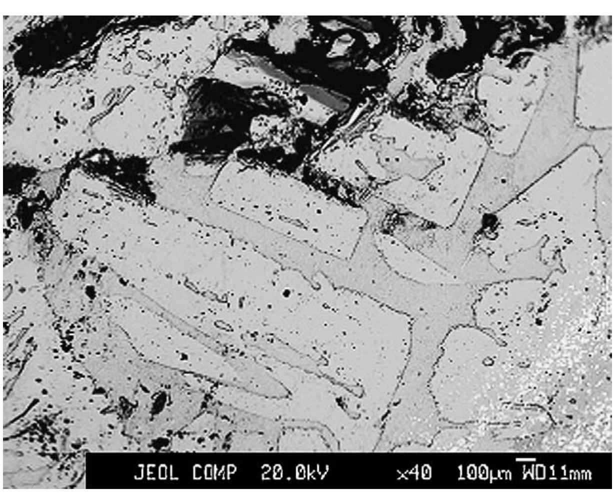

Fig. 5. Micrograph of specimen no. 25 (annealed at 873 K) in characteristic X-rays. The rectangular crystals are of Ti_2Zn_3. The composition of the matrix phase is close to the formula $TiZn_8$.

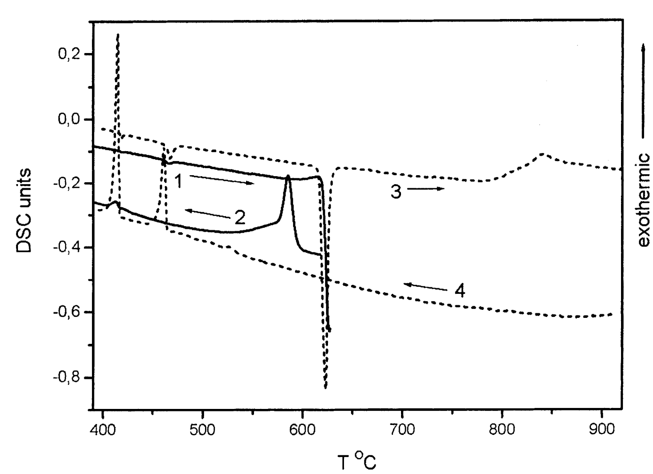

Fig. 7. Thermal curves of specimen no. 27 (X_{zn} = 0.885; mass = 34.2 mg). Curve 1-heating up to 630 °C (first cycle), 2-cooling down to 380 °C (first cycle), 3-(dashed line) heating up to 920 °C (second cycle), 4-(dashed line) cooling down to 380 °C (second cycle). The temperature (°C) is plotted along the abscissa, and DSC units (mW)–along the ordinate. The endothermic peaks show downward.

while the main layer appertains to $TiZn_3$ (Fig. 4). Along the wall of the silica tube a layer with approximate composition Ti_5SiZn_4 has formed. Nevertheless Si has not been found inside the volume of the studied diffusion couple.

In many alloys (nos. 1, 3, 5, 7, 10, 11, 20, 24–26, see Tables 2–5) crystals corresponding to the formula Ti_2Zn_3 (Fig. 5) have been observed as well.

The growth of the reactionary diffusion layers (at constant temperature and pressure) depends on two processes (assuming infinitely fast nucleation rate): the diffusion and the interface chemical reaction, because each of them proceeds at a final rate. As known, in case of consecutive processes, the slowest one is rate controlling. Thus at one limit, it can be the diffusion (then a parabolic growth is expected) and on the other limit, it is the chemical reaction rate (then a linear growth is expected) [31–34]. In the case of solid/liquid diffusion layers the dissolution rate of the solid also affects the total layers thickness.

In this work, constant (linear) growth rates have been found (Fig. 6). The total thickness (Δx) of a diffusion layer represents the mean value of 10 measurements. Nevertheless, due to the porosity and the roughness of the outer layer (adjacent to the liquid phase) we assume that an error of around 10% can be attributed to Δx.

The growth rate constants calculated from our data are $(7.5 \pm 0.3) \times 10^{-9}$ and $(8.0 \pm 0.2) \times 10^{-9}\,\mathrm{m\,s^{-1}}$, at 500 and 600 °C, respectively.

The straight lines in Fig. 6 appear to cross the abscissa at negative times. However, one should be aware that at the very beginning of the reaction, the effective growth rates are faster and after some time they slow down [34]. The dissolution of the reaction layer in the undersaturated zinc melt has a similar effect [31,32]. Consequently, the growth rates calculated above are not valid at very small reaction times.

Also we have found that for 30 min at 500 °C and for 15 min at 600 °C continuous reaction layers could not form.

3.3. Thermochemical studies

Differential scanning calorimetry (DSC) analyses have been performed using NETZSCH DSC 404C instrument. For this purpose an alloy with known composition (determined by AES-ICP analyses—$X_{Zn} = 0.885 \pm 0.001$) has been powdered and sealed under vacuum in silica capsule. Heating and cooling cycles have been performed in steady-state pure Ar flow. Isothermal heating (3 min) has been applied between the dynamic sections in order to smooth the transition from one to another heating rate. Pure metals have been used in order to check up the temperature calibration of the instrument.

DSC curves of this specimen (no. 27) are shown in Figs. 7, 8A and B. The strongest endothermic peak is at about 611 °C (Fig. 8A). We attribute it to the peritectic melting of the $TiZn_7$. As this peak is large it is possible also that it reflects the melting of the phase $TiZn_5$ (i.e. the melting temperatures of the two latter compounds are near). This hypothesis is confirmed by the cooling curve where two peaks are distinguishable (Fig. 8A).

The peak, corresponding to the $TiZn_3$ melting, is expected at about 900 °C [16]. Nevertheless it could not be observed even until 920 °C (Fig. 7). It is possible that the $TiZn_3$ melting point is situated at a higher temperature or that it is masked by the chemical interactions between Ti and SiO_2 occurring also near to this temperature. Due to the latter interactions some quantity of Ti is extracted from the specimen, thus its composition shifts toward the Zn side.

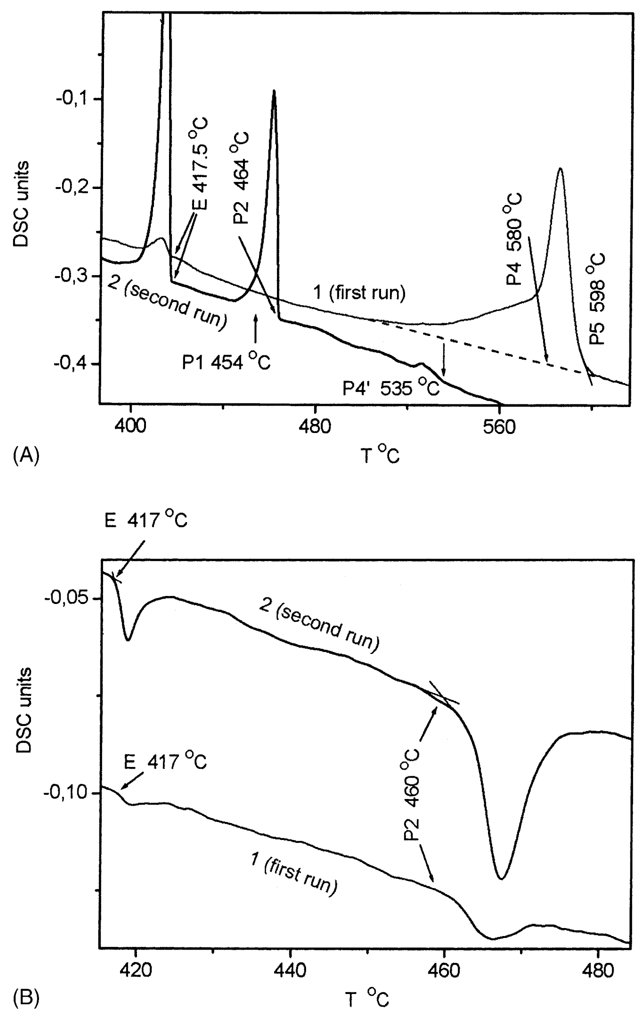

Fig. 8. (A) DSC curves (at cooling) obtained with material of specimen no. 27. Curves 1 and 2 show data of the first and second run ($10\,\mathrm{K\,min^{-1}}$), respectively, Peaks' signification: E-eutectic invariant; P1-peritectic crystallization of $TiZn_{16}$; P2-peritectic crystallization of $TiZn_{10}$; P4-peritectic crystallization of $TiZn_7$; P4′-probably formation of $TiZn_7$ from supercooled liquid; P5-probally formation of $TiZn_5$. (B) DSC curves (at heating) of specimen no. 27. Heating rate $10\,\mathrm{K\,min^{-1}}$. The curve 1 is registered during the first run, and curve 2–during the second run. The temperature (°C) is plotted along the abscissa, and DSC units (mW)–along the ordinate. Peaks' signification: E–eutectic invariant; P2–peritectic melting of $TiZn_{10}$.

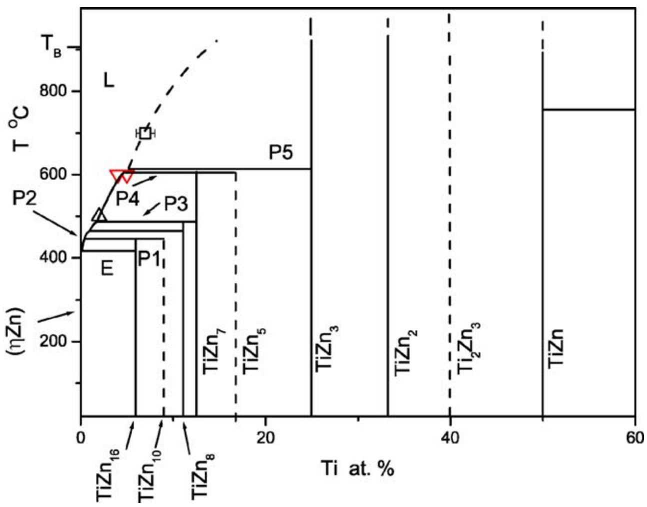

Fig. 9. Zinc-rich side of the Ti–Zn Phase diagram. The invariants denoted with the letters E, P1–P5 correspond, respectively, to the following temperatures: 418.6, 446, 468, 486, ∼609, ∼615 °C; P6-peritectoid invariant ($Ti_2Zn \leftrightarrow TiZn + (\beta Ti)$); T_B–Zn boiling point. The dashed lines show phases or phase boundaries the most liable to more accurate specification; liquidus points: Δ–this work, 500 °C, X–this work, 600 °C, −700 °C, Vassilev [26].

As consequence, at cooling two other invariants are crossed (Fig. 8A)—one is the eutectic line ($T \approx 419\,^\circ C$), while the other ($T \approx 460\,^\circ C$) could be attributed [26] to the peritectic reaction: $Liq + TiZn_8 \leftrightarrow TiZn_{10}$.

Finally, taking into account the results reported in this work as well as our other studies [26] and literature data [4,16,21] we constructed new design of the phase equilibria in the zinc-rich region of the Ti–Zn system (Fig. 9). In this figure dashed lines represent the argued compounds $TiZn_5$ and $TiZn_{10}$ because their existence and composition could not be confirmed by the electron microscope studies. Nevertheless, some thermal arrests (P2 and P5) might be associated with these phases (Fig. 8A and B). There are other studies confirming the presence of six thermal peaks in the Zn-rich side of the Ti–Zn system [18]. Thus the existence of the $TiZn_{10}$ and $TiZn_5$ phases cannot be completely denied, although they might have compositions differing from the present formulae. That is why we prefer keeping them (although under question) in the phase diagram attracting in this way further investigations to resolve this problem.

The liquidus points obtained in this work have been used for the estimation of the enthalpy of dissolution of Ti into molten Zn($\Delta\overline{H_{Ti}}$). For this purpose $\ln(X_{Ti}^{Liq})$ has been plotted against the reciprocal temperature. The slope of the calculated line represents [30] the ratio $-\Delta\overline{H_{Ti}}/R$ (R is the universal gas constant and X_{Ti}^{Liq} is the Ti mole fraction of the liquidus points). Thus a value of around $40\,kJ\,mol^{-1}$ has been evaluated for $\Delta\overline{H_{Ti}}$. It differs greatly from the assessment [29] done by the Miedema model for the pertinent enthalpy of solution at infinite dilution ($-61\,kJ\,mol^{-1}$).

4. Conclusion

The Ti–Zn phase diagram and the layers growth kinetics in this system have been studied. Linear time dependence has been found for the Ti–Zn layers grown at 500 and 600 °C. The pertinent growth constants have been calculated. The adhesion of the reactionary layers one to another as well as to the titanium is feeble. That is why, they often break and separate, thus giving place to very fast reaction between both metals.

It seems that Ti–Zn phases could exist (probably in metastable state) out of their respective exact stoichiometry. The formation of some metastable compounds could not be excluded either.

Significant metastable homogeneity ranges have been observed for some phases. For example $TiZn_3$ appears in an interval of 70–80 at.% Zn. There are indications about the existence of a formerly unknown compound containing around 60 at.% Zn (Ti_2Zn_3).

The peritectic temperatures of the phases $TiZn_7$ and, probably, $TiZn_8$ are near one to another, while no other endothermic thermal arrest (for example of $TiZn_3$) has been observed until 920 °C.

Acknowledgements

One of the authors (G.P.V.) gratefully acknowledges the support of the Japanese Society for Promotion of Science. Thanks are due also to Mr. Takaku (Tohoku University, Sendai, Japan) for technical assistance with electron microprobe analyses.

References

[1] G.L. Leone, P. Niessen, H.W. Kerr, Metall. Trans. B 6 (1975) 503.
[2] G.L. Leone, H.W. Kerr, J. Cryst. Growth 32 (1976) 111.
[3] S.H. Jeon, Han'guk Pyomyon Konghak Hoechi 30 (1997) 320 (in Korean).
[4] T. Gloriant, G. Reumont, P. Perrot, Z. Metallkd. 88 (1997) 539.
[5] G. Reumont, T. Gloriant, P. Perrot, J. Mater. Sci. Lett. 16 (1997) 62.
[6] G.P. Vassilev, E.S. Dobrev, J.-C. Tedenac, T. Czeppe, in: Proceedings of the VIIIth Seminar on Diffusion and Thermodynamics of Solids, 4–6 September 2002, Brno, Czech Republic.
[7] M. Hansen, K. Anderko, Constitution of Binary Alloys, second ed., McGraw-Hill, New York, 1958, p. 1488.
[8] J. Murray, Bull. Alloy Phase Diagrams 5 (1) (1984) 52.
[9] B. Predel, in: O. Madelung (Ed. in Chief), Phase Equilibria, Crystallographic and Thermodynamic Data of Binary Alloys, vol. 5, subvol. b, Springer-Verlag, Berlin, 1992, pp. 295–296.
[10] T. Massalski, CD ROM: Binary Alloy Phase Diagrams, ASM International, OH, USA, 1996.
[11] E. Gebhardt, Z. Metallkd. 33 (1941) 355.
[12] E.A. Anderson, E.J. Boyle, P.W. Ramsey, Trans. Am. Inst. Mining, Metall. Petrol Eng. 156 (1944) 278.
[13] P. Pietrokowsky, Trans. AIME 200 (1954) 219.
[14] K. Schubert, K. Frank, R. Gohle, A. Maldonado, H.G. Meissner, A. Raman, W. Rossteutscher, Naturwissienschaften 50 (1963) 41.
[15] M.E. Pelzel, Metallography 15 (1961) 881.

[16] W. Heine, U. Zwicker, Z. Metallkd. 53 (1962) 380.
[17] W. Piotrowski, Zeszyty Nauk. Politech. Lodz. Mech. 10 (1963) 33 (in Polish).
[18] E.H. Rennhack, Trans. Metall. Soc. AIME 236 (1966) 941.
[19] J.A. Spittle, Metallography 5 (1972) 423.
[20] S. Goto, K. Esashi, S. Koda, S. Morozumi, J. Jpn. Inst. Met. 37 (1973) 466.
[21] S. Ono, H. Ohtani, M. Hasebe, in: Proceedings of 9th Symposium on Microjoining and Assembly Technology in Electronics, Yokohama, Japan, 6–7 February 2003.
[22] Powder Diffraction Files, JCPDS-ICDD, CD-ROM, 1995.
[23] P. Villars (Ed. in Chief), Pauling File Binaries Edition, Inorganic Materials Database and Design System, CD-ROM, Germany, ISBN 3-00-009043-6.
[24] M. Saillard, G. Develey, C. Becle, J.M. Moreau, D. Paccard, Acta Crystallogr. B37 (1981) 224.
[25] X.-A. Chen, W. Jeitschko, M. Danebrock, Ch. Evers, K. Wagner, J. Solid State Chem. 118 (1995) 219.
[26] G.P. Vassilev, E. Dobrev, Contribution to the zinc-rich side of the Ti–Zn system, in preparation.
[27] F. Laves, H. Wallbaum, Naturwissenschaften 27 (1939) 674.
[28] W. Rossteutscher, K. Schubert, Z. Metallkd. 56 (1965) 730.
[29] A.K. Niessen, F.R. de Boer, R. Boom, R.F. de Chatel, W.C.M. Mattens, A.R. Miedema, CALPHAD 7 (1983) 51.
[30] R. Swalin, Thermodynamics of Solids, Wiley, New York, London, 1961.
[31] V. Dybkov, J. Mater. Sci. 21 (1986) 3078.
[32] V. Dybkov, J. Mater. Sci. 21 (1986) 3085.
[33] J.S. Kirkaldy, D.J. Young, Diffusion in the Condensed State, The Institute of Metals, London, 1987, p. 527.
[34] F.J.J. van Loo, Prog. Solid State Chem. 20 (1990) 47.